Patterning

Structure Formation by Dynamic Self-Assembly

Liqiang Li, Michael H. Köpf, Svetlana V. Gurevich, Rudolf Friedrich, and Lifeng Chi**

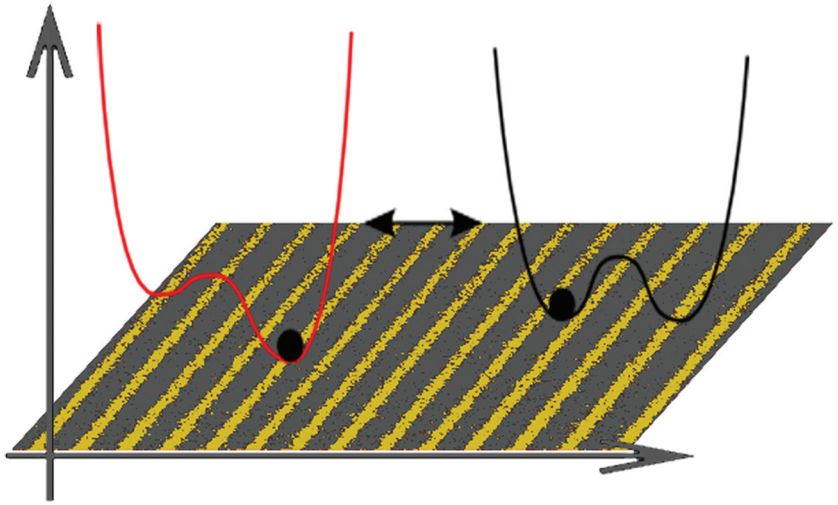

From the Contents

This review summarizes the work conducted in the last decade on the fabrication of mesostructured patterns, which have lateral dimensions within the nano- and microscales, over a wafer-scaled size by means of dynamic self-assembly using Langmuir–Blodgett (LB) transfer or dip-coating. First, strategies to form mesostructures from a homogeneous Langmuir monolayer with controlled shape, size, and patterns alignment will be presented, followed by a detailed theoretical explanation of the pattern formation. In addition, the patterning of nanocrystals and other chemicals with LB transfer or other dynamic processes, such as dip-coating, will be summarized.

small NANO MICRO

1. Introduction

Surface patterning has become an important part of modern science and technology, especially in the areas of micro-electronics, information processing and storage, nano-/microfluidic devices, and biodection.[1,2] The formation of patterned surfaces is also an ubiquitous and fascinating phenomenon in nature; as examples we mention regular stripes on the zebra's surface or the wings of butterflies.[3] Fabrication and investigation of patterned surfaces are active areas of research in chemistry, physics, materials science, and biology. Methods used for pattern fabrication are commonly characterized as "top-down" and "bottom-up". In the top-down approach, the features are written directly or transferred onto a substrate, e.g., by optical and e-beam lithography, and then the microscopic and/or nanoscopic features are engraved by applying appropriate etching and deposition processes. Although there is much focus on overcoming practical limits in fabricating small features,[4] another important limit is how large of an area can be efficiently patterned with small features. This limit arises because in order to write small features, it is necessary to focus on a smaller surface area.[5] The concepts of self-assembly and self-organization provide an alternative approach to realize small features over large areas via bottom-up approaches,[6] which rely on the interactions of building blocks such as molecules or nanoparticles that spontaneously assemble into nano-/microstructures. The self-assembly and self-organization processes as well as the characteristics of the surface patterns (e.g., shape, size, function) can be controlled by tailoring the properties of building blocks. Self-assembly processes are mainly classified as static self-assembly and dynamic self-assembly (similar to self-organization). By definition, self-assembly refers to autonomous organization of components into structures under defined boundary conditions.[7] Self-organization (a term originating from biology) is a mechanism for the formation of patterns, processes, and structures at a higher level through multiple interactions among the components at the lower level, which are mainly based on weak interactions between the molecules.[7] Dynamic and nonlinear effects are often characteristic in self-organization processes. While the current understanding of self-assembly comes from the examination of static systems, mechanistic details of dynamic self-assembly are much less addressed.

The Langmuir–Blodgett (LB) technique is a well-established and sophisticated method to control interfacial molecular orientation and packing.[8–10] Moreover, it is an efficient approach towards the controllable fabrication of laterally patterned structures on solid supports, termed LB patterning. Laterally nanostructured LB monolayers are normally generated by the deposition of ordered 2D structures formed at the air–water interface onto solid substrates.[11–14] Alternatively, the LB transfer process itself can be used to form patterns near the three-phase contact line from a homogeneous Langmuir monolayer.

This review intends to provide a comprehensive summary of surface patterning during LB transfer, a typical dynamic self-assembly or self-organization process. The lateral patterning in LB monolayer prepared at the air–water interface and consequently transferred onto a solid substrate will not be the focus of this review. We will review here the work conducted in the last decade in the fabrication of mesostructured patterns, which have lateral dimensions within the nano- and microscales, over a wafer-scaled size using the LB technique. First, strategies to form mesostructures from a homogeneous Langmuir monolayer with controlled shape, size, and pattern alignment will be presented. A detailed theoretical explanation will be outlined in Section 3, and lastly, the patterning of nanocrystals and other chemicals with LB transfer or other dynamic processes such as dip-coating will be presented.

2. Fabrication of Controllable Mesostructures Based on Lipids

DPPC, one of the major lipid components of biological membranes, shows a typical phase behavior of a Langmuir monolayer at the air–water interface, characterized by a liquid-expanded (LE) phase, a liquid-condensed (LC) phase, and a LE–LC phase transition, confirmed by the (surface pressure)–(molecular area), π–A, isotherm and Brewster angle microscopy (BAM) images (**Figure 1**).[15,16] In the LE phase, the DPPC monolayer behaves as a quasi-2D liquid,

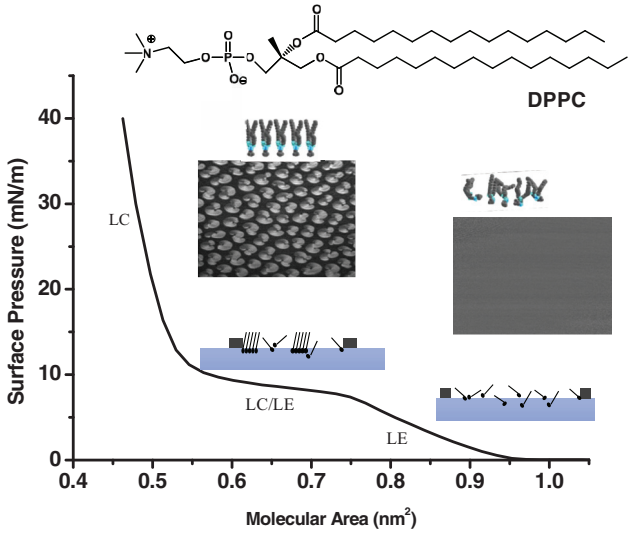

Figure 1. Phase behavior of the DPPC monolayer at the air–water interface. Top: chemical structure of DPPC. Bottom: π–A isotherm of DPPC (~23 °C) and typical BAM images (430 μm × 537 μm) for the LE phases and LE–LC phase transition along with the corresponding conformations of the DPPC molecules. Reprinted with permission.[81] Copyright 2007, American Chemical Society.

Dr. L. Q. Li, Prof. L. F. Chi
Physikalisches Institut
Universität Münster
Wilhelm-Klemm-Str. 10, Münster 48149, Germany
E-mail: chi@uni-muenster.de
Dr. M. H. Köpf, Dr. S. V. Gurevich, Prof. R. Friedrich
Institut für Theoretische Physik
Universität Münster
Wilhelm-Klemm-Str. 9, Münster 48149, Germany
E-mail: fiddir@uni-muenster.de

DOI: 10.1002/smll.201101930

where the head groups of the DPPC molecules are translationally disordered and chains are conformationally disordered. Upon decreasing of molecular areas, DPPC molecules begin to condense and a co-existing phase of LE and crystalline LC occurs at the plateau region of the isotherm. Finally a homogeneous well-packed condensed monolayer (LC phase) appears at smaller molecular areas.

2.1. Formation of Mesostructures with Nanochannels

The fabrication approach using the LB transfer process to create mesoscopic patterns is based on the work of H. Riegler in the early 1990s.[17,18] He first reported the transfer induced phase transitions (i.e., substrate-mediated condensation) near the three-phase contact line from a homogeneous DPPC Langmuir monolayer in the LE phase. The resulting stripe formation had a typical size scale in micrometers.[17,18] Intriguingly, by elevating the transfer speed, alternating stripes with widths of approximately 800 nm separated by channels of about 200 nm in width were obtained, as detected by atomic force microscopy (AFM, **Figure 2**b).[19] Although directly observing the stripe formation in situ at the three-phase contact line in this system is difficult, one can imagine the process as depicted in the schematic illustration of Figure 2a. The height difference between the stripes and channels is about 1 nm, as measured by AFM, with the stripes composed of condensed (LC phase) DPPC molecules. Considering that the length of a DPPC molecule is about 2 nm, the material in the channels is attributed to the expanded (similar to LE phase) DPPC molecules, which have a larger tilt angle compared with condensed DPPC molecules in the stripes (Figure 2c). This was confirmed through dynamic force spectroscopy measurements, where accurate detection of the tip–sample interaction forces is possible to distinguish different phases.

In this system, the size, orientation, and shape of DPPC patterns can be controlled by adjusting experimental conditions such as the transfer velocity, surface pressure, subphase temperature, substrate chemistry, monolayer composition, humidity, and the transfer method. This tunability is essential to realizing applications in surface patterning.

2.2 Effect of Surface Pressure and Transfer Velocity

The lateral size and orientation of the DPPC stripe pattern from the pure DPPC monolayer strongly depends on the transfer surface pressure and transfer velocity.[20,21] For instance, on mica substrates, at a surface pressure of 3.0 mN/m, a high transfer velocity of 60 mm/min induces the formation of horizontal DPPC stripes parallel to the three-phase contact line (**Figure 3**a,d). In contrast, vertical stripes perpendicular to the three-phase contact line (Figure 3c,f) are obtained at a low transfer velocity (10 mm/min). A very similar switching of the direction of stripe patterns during LB transfer was reported by Pignataro and co-workers using a slightly shorter phospholipid, L-α-dimyristoylphosphatidylcholine (DMPC).[22] In the DPPC system, a grid pattern, clearly showing the superposition of horizontal stripes and vertical stripes, is observed at a transfer velocity of 40 mm/min (Figure 3b). In general, horizontal stripes only appear at the high transfer velocity (60 mm/min) with low transfer surface pressure, and the pure vertical stripes only appear at the low transfer velocity and high transfer surface pressure (still in LE phase). It is also generally true that the faster the transfer speed, the smaller the features.

2.3. Effect of the Substrate

Different hydrophilic substrates can be used to obtain DPPC mesostructures; however, the experimental conditions for pattern formation are different due to the different surface properties. One component of the stripe pattern formation is the substrate-mediated condensation of DPPC during the LB transfer; as such, the molecule–substrate interaction should be a very important factor in this self-organization process. For instance, the periodic stripe patterns can be formed on oxygen plasma-treated silicon surface, but the transfer velocity is slower than the velocity with a mica surface at

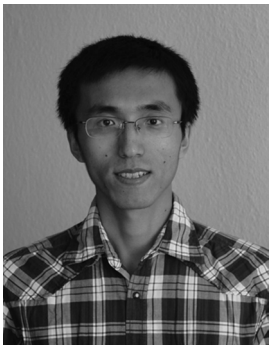

Liqiang Li received his Ph.D. in physical chemistry from the Institute of Chemistry, Chinese Academy of Sciences, in 2008. Since then, he has been working as a postdoctoral follow in the Physical Institute of Münster University in Germany. His research interests focus on the assembly and patterning of organic functional materials including insulators, semiconductors, and conductors, and their applications in opto-electronic devices (mainly organic thin-film transistors).

Michael H. Köpf obtained his Ph.D. in 2011 from the Institute for Theoretical Physics at the University of Münster, Germany. Since 2008, he has been investigating the nanoscopic pattern formation in the controlled dewetting of complex fluids. Currently, he is a postdoctoral fellow at the Technion-Israel Institute of Technology in Haifa, Israel. He works on pattern formation phenomena with a special focus on complex fluids, soft matter, and active biomaterials.

Svetlana V. Gurevich graduated with an applied mathematics degree from the Saint-Petersburg State University, Russia, in 2002, and she obtained her Ph.D. in physics (2007) in the group of Prof. H.-G. Purwins at the University of Münster, Germany, working on the theoretical description of self-organization processes in gas-discharge systems. Since 2007, she has been working as a postdoctoral fellow in the group of Prof. Friedrich at the University of Münster. Her research interests are focused on the fundamental aspects of the theory of complex systems such as localized structures and pattern formation in thin films.

small NANO MICRO

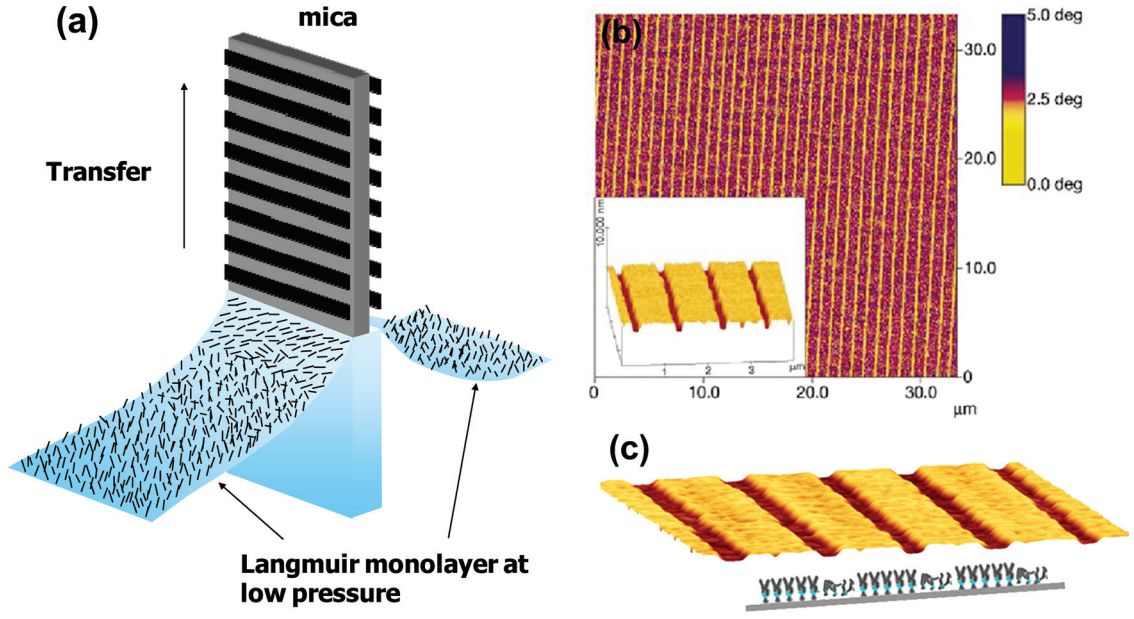

Figure 2. a) Schematic illustration of the process of mesopattern formation. b) Mesostructures with nanochannels on mica in phase (main figure) and topography (inset) imaging. Experimental conditions: surface pressure, 3 mN/m; transfer velocity, 60 mm/min; and temperature, 22.5 °C. c) The composition of DPPC pattern: the DPPC stripe pattern is composed of expanded DPPC molecules in the channels and condensed DPPC molecules in the stripes. Reprinted with permission.[81] Copyright 2007, American Chemical Society.

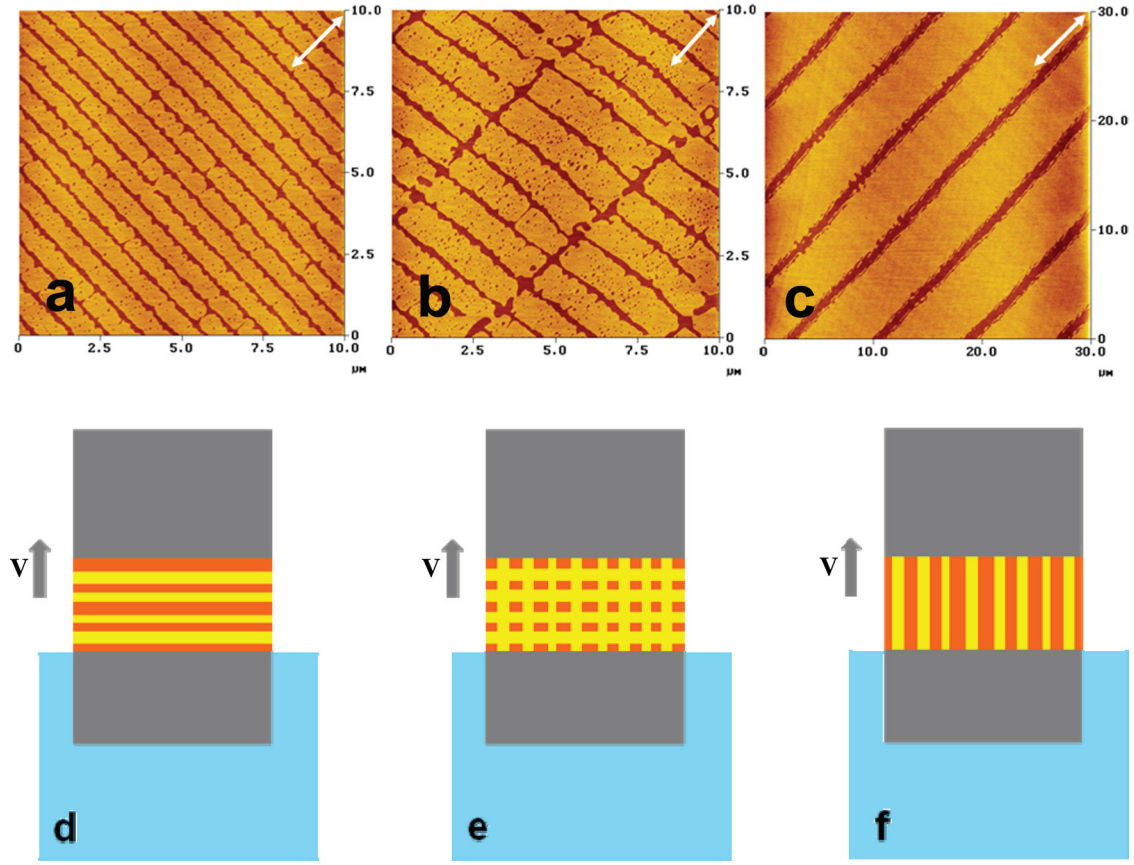

Figure 3. The shape and alignment of patterns (pure DPPC) depending on the transfer conditions. a–c) AFM images of the various pure DPPC patterns on mica surfaces. a) 60 mm/min and 3 mN/m, b) 40 mm/min and 3 mN/m, and c) 10 mm/min and 3 mN/m. Double arrows in the AFM images shows the axis of film transfer. d–f) Schematic illustration for the formation of various patterns during the LB vertical deposition. Reprinted with permission.[81] Copyright 2007, American Chemical Society.

the same surface pressure and temperature.[23] Moreover, different treatments of the silicon substrate will affect the DPPC pattern formation. At the same transfer velocity, the surface pressure for forming stripe patterns on RCA-treated (a 5:1:1 mixture of $H_2O/H_2O_2/NH_4OH$ at 70 °C) silicon wafers is higher than for that on oxygen plasma-treated silicon wafers.[24] One possible reason is due to the different interfacial energies of RCA-treated silicon wafer (106 ± 3 mJ/m^2) and oxygen plasma-treated silicon wafer (88 ± 2 mJ/m^2). Another one is due to the different Si–OH group concentration on the wafer surfaces, which is an important factor for the substrate-mediated condensation of DPPC molecules during the draining process of water on the substrate.[25] The concentration of Si–OH on RCA-treated silicon wafer is 34% higher than that on an oxygen plasma-treated silicon wafer. The substrate roughness, which may influence the kinetics of the DPPC phase transition and dynamic contact angle of meniscus at the three-phase contact line, is likely to be another factor to influence the pattern formation, although this parameter has not yet been systematically studied.

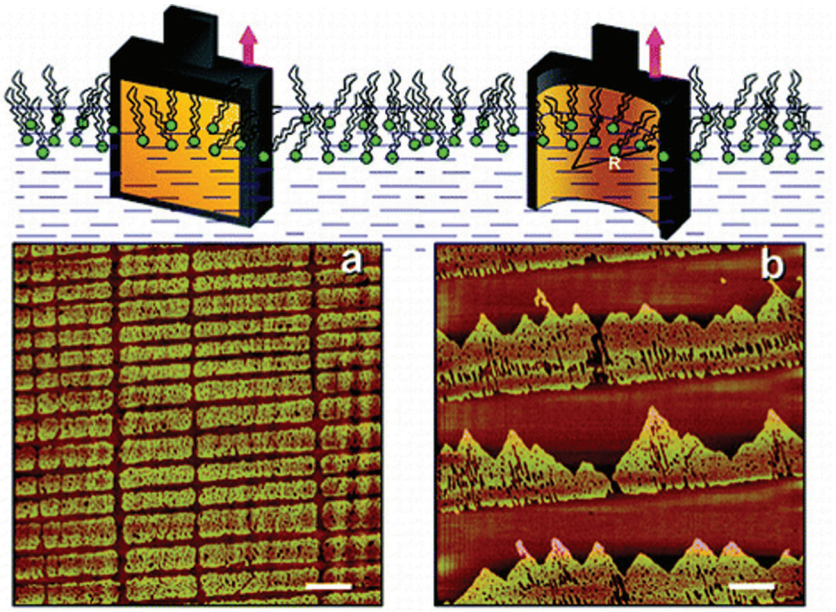

Figure 4. Schematic display of LB transfer of DPPC monolayer onto macroscopically curved mica surfaces and flat mica substrate. Differences are revealed by AFM images: a) on flat mica surface and b) on curved mica surface. Surface pressure: 2 mN/m. Transfer speed: 20 mm/min. Scale bar: 5 μm. Reprinted with permission.[26] Copyright 2007, American Chemical Society.

It is interestingly to note that by using a curved surface (e.g., mica), instead of the flat surface, the microscopic patterns are different. Fischer and co-workers demonstrated that, on the curved surface, a modulated horizontal striped pattern evolved to a zigzag boundary at the LC front of the stripe and a continuous straight boundary at the LC rear (**Figure 4**).[26] They proposed that the sensitivity of the pattern to the macroscopic curvature of the substrate is due to a flow-controlled hydrodynamic instability from the subphase flow near the three-phase contact line.

2.4 Effect of the Second Component

For a mixed monolayer, the miscibility of various components is important to the phase behavior and the stability of the monolayer. To study this effect on the pattern formation, an additive component, 1,2-di(2,4-octadecadienoyl)-*sn*-glycero-3-phospho-choline (DOEPC), was selected for use with the DPPC, since DOEPC has a similar molecular structure to DPPC and yet forms a fully LE phase at the air–water interface under the same conditions. Compared with the pure DPPC monolayer, the mixed monolayer of DPPC/DOEPC (1:0.1) shifts the pattern formation to lower velocities and higher surface pressures, with the increased ability to form horizontal stripes.[20] The grid pattern only appears at low transfer velocity (1 mm/min) and high transfer surface pressures. Generally, the size of stripes in the mixed DPPC/DOEPC (1:0.1) patterns is ca. 4–6 times smaller than that of stripes formed by a pure DPPC monolayer at the same transfer conditions.[20]

2.5 Gradient Mesotructured Surface by LB Rotating Transfer

Based on the transfer velocity dependent pattern formation,[20,27] a simple yet novel method was further developed, LB rotating transfer, to achieve a gradient mesostructure in a well-ordered fashion over large areas.[28] The conventional vertical dipper is only able to move the substrate up or down normal to the water surface during the film transfer, with the linear velocity for all points on the substrate constant. During LB rotating transfer, however, the floating monolayer at the air–water interface is transferred onto the substrate by rotating the substrate along the x-axis (**Figure 5**a), with the linear velocity at different points on the substrate depending on the distance to the axis of rotation as shown in the simulation results (Figure 5b). As a result, LB patterns with different dimensions and orientations (white lines in Figure 5b) that depend on the transfer velocity can be generated simultaneously. Figure 5c shows fluorescence micrographs of gradient stripe patterns along the red line (middle line of the substrate) in Figure 5b, which is formed by LB rotating transfer of a mixed monolayer of DPPC and a fluorescence dye NBD (2-(12-(7-nitrobenz-2-oxa-1,3-diazol-4-yl)-amino)dodecanoyl-1-hexadecanoyl-*sn*-glycero-3-phosphocholine, 2 mol%) (rotational frequency, $\omega = 0.07$ rpm; surface pressure, $\pi = 2$ mN/m). The angle between the red line and the three-phase contact line decreases with increasing radius, which fits well to the theoretical expectation (Figure 5d). Moreover, the lateral width of the luminescent stripe and the periodicity strongly depend on the radius: mono-exponentially decreasing with increasing radii, as shown in Figure 5e. It is easy to extrapolate the ideas presented here to other systems, such as nanoparticles[29,30] and lipid/lipopolymer,[31] to obtain complex arrays, and test the experimental conditions for exploring the pattern formation (i.e., high-throughput studies).

small NANO MICRO

3. Theoretical Model of Pattern Formation During Monolayer Transfer

The experimental observations show that the stripe pattern formation during LB transfer is directly related to the thermodynamics of the monolayer in the vicinity of the LE–LC phase transition. As the density of the monolayer varies significantly between the LE and LC domains comprising the stripes, the theoretical description of their formation dynamics has to include the dependence of the surface pressure on the surfactant density; that is, it has to include the monolayer's equation of state. In that respect, the problem under consideration has to be distinguished from the stripe pattern formation observed by Mahnke et al. and Kurnaz et al. in LB films of fatty acids that were already condensed before the transfer and that exhibit a meniscus instability due to concentration polarization.[32,33] Instead of alternating thermodynamic phases they observe alternating stripes of arachidic acid and cadmium arachidate perpendicular to the transfer direction and the surface pressure remains constant throughout the transfer. For a theoretical discussion of these phenomena, the reader is referred to the articles by Kovalchuk et al.[34–36]

Here, we follow the approach to link the surfactant thermodynamics to the subphase hydrodynamics via the surface tension which is directly related to the surface pressure by the equation $\sigma = \sigma_0 - \pi$, where σ is the actual surface tension of the surfactant-contaminated film and σ_0 is the surface tension of clean water.[37] As can be seen from the pressure–area isotherms the surface pressure close to the phase transition depends on the surfactant density in a strongly nonlinear way (see **Figure 6**). The theoretical description of this dependence is outlined in the following section.

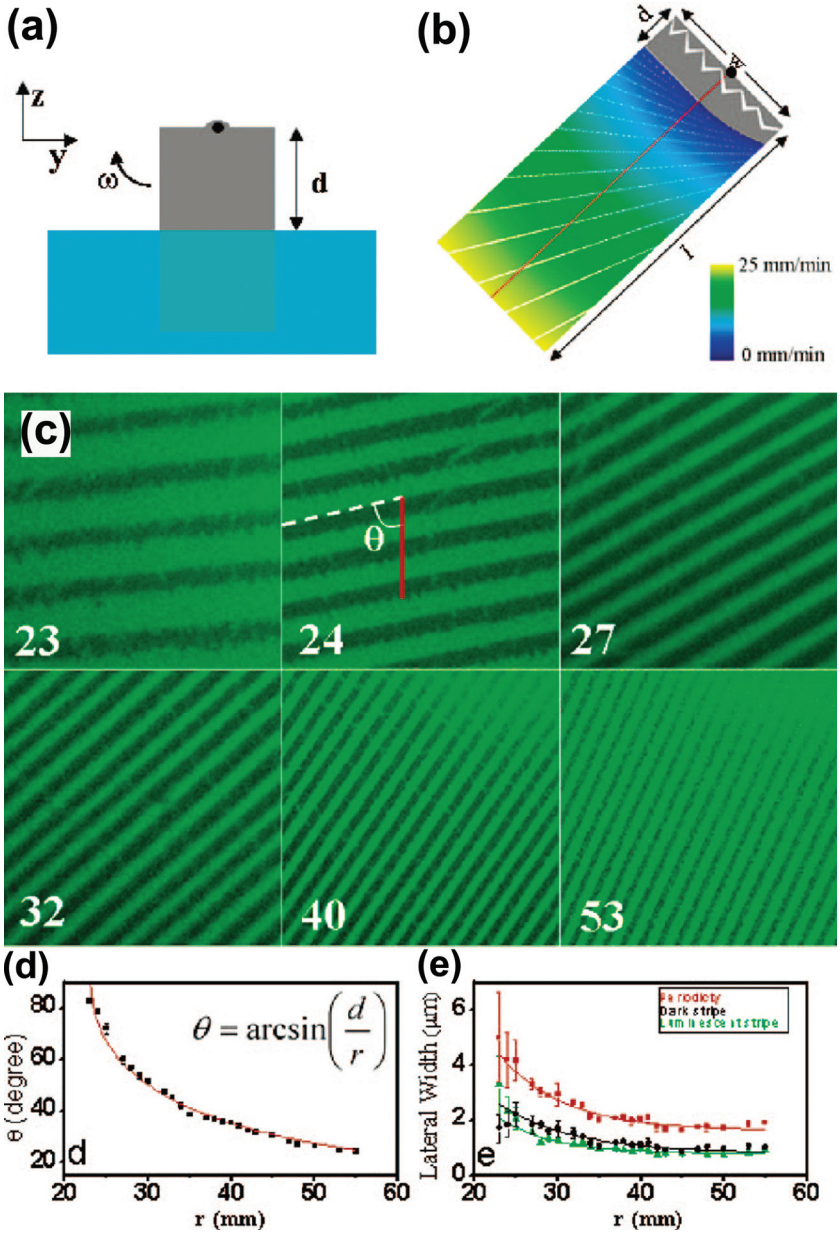

Figure 5. a) Schematic illustration of LB rotating transfer. b) Simulated distribution of the linear velocity perpendicular to the three-phase contact line (v_v) and orientation (denoted by white lines) of the stripes; depth, $d = 23$ mm; frequency rotation, $\omega = 0.07$ rpm; length, $l = 60$ mm; and width, $w = 20$ mm. c) Fluorescence images (30 μm × 30 μm) of the pattern at various points along the red line in (b). The number in each image is the radius (r, mm), and the dotted line is parallel to the three-phase contact line. d) The dependence of θ on the radius, which could be fitted well (red line, $r^2 = 0.98$) by the theoretical equation. e) The dependence of the lateral width of luminescent stripe (green), dark stripe (black), and periodicity (red) of gradient patterns on the radius. All data in (e) are fitted by a mono-exponential decay. Reprinted with permission.[81] Copyright 2007, American Chemical Society.

3.1. Monolayer Thermodynamics and Substrate-Mediated Condensation

Mono- and multilayers of surfactants at the free water–air interface are known to exhibit complicated thermodynamic properties and extremely rich phase diagrams.[16] As the present review is concerned with the formation of LE–LC stripe patterns, we will focus on the vicinity of the LE–LC phase transition, a regime in which the monolayer can be described reasonably well by a scalar field γ representing the surfactant number density. In order to describe the abundant different ordering states found in Langmuir monolayers far away from the main transition, it is necessary to take into account also the orientation of the molecules. Theoretical approaches to these problems can be found in the review by Kaganer et al..[38] The characteristics of the thermodynamic properties of a surfactant monolayer close to the LE–LC phase transition is captured by its surface pressure isotherm that determines the monolayers' equation of state $\pi = \pi(\gamma)$,

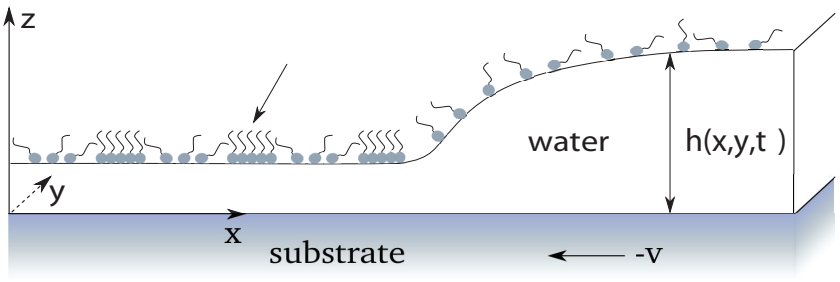

Figure 6. The surfactant-covered liquid thin film is described by means of the height profile h (x,y,t) that indicates the film thickness above the point (x,y) on the substrate and the surfactant number density γ (x,y,t) at the surface above (x,y); t represents time. Reprinted with permission.[62] Copyright 2010, American Chemical Society.

that is the dependence of the surface pressure on the surfactant density. In the vicinity of the main transition, this equation of state can be written in the form

$$\pi(\gamma) = -\kappa\left((\nabla\gamma)^2\,(\gamma + \gamma_{cr})\,\Delta\gamma\right) + \pi_{hom}(\gamma) \quad (1)$$

where κ denotes the coefficient of line tension between domains of different densities. The surface pressure of a homogeneous system, i.e., a system without density variations $\pi_{hom}(\gamma)$, can be approximated by a third order polynomial centered around the critical density γ_{cr} of the LE–LC phase transiotion.This formula can be derived rigorously from a free-energy functional of the type proposed by Cahn and Hilliard for continuous inhomogeneous systems.[39,40] The resulting isotherm of a homogeneous monolayer then has the typical S-shape known from the van-der-Waals theory of real gases.[41] Because of phase-coexistence within the binodal region, one has to apply Maxwell's construction to obtain the horizontal part of the isotherm as a valid description of nonhomogeneous equilibrium states. In other words, the monolayer is considered as a 2D real gas similar to the van-der-Waals gas.

The stripe patterns obtained in LB transfer experiments consist of alternating domains of the LE and the LC phases. It is therefore particularly remarkable that these structures result from transfer of a monolayer which is prepared in the pure LE phase on the water surface in the Langmuir trough. This means that the surface pressure is well below the LE–LC coexistence pressure throughout the whole transfer process. Obviously there has to be some mechanism which induces a partial condensation of the LE layer during the transfer onto the substrate. This effect is known as substrate-mediated condensation (SMC) in the literature and is attributed to an interaction between the substrate and the monolayer.[17,18,42–45] To be more specific, this interaction lowers the free energy of the LC phase when the monolayer comes closer to the substrate.[17] By this mechanism, the LC phase is energetically favored at the substrate and the condensation is facilitated.

The interaction can be modeled using an interaction field, s, whose strength depends on the distance between substrate and monolayer, which in our case is just given by the thickness h of the water film in between. This field is introduced into the surfactant thermodynamics as an external field, resulting in a modified surface pressure of the form

$$\pi^{(SMC)}(\gamma) = \pi(\gamma) + s(h) \quad (2)$$

For small values of h, when the monolayer is close to the surface, the external field yields a tilt of the free energy towards its higher density minimum, that corresponds to the pure LC phase. Accordingly, the system favors the LC state energetically in the vicinity of the substrate, thereby facilitating the condensation of the monolayer.

Although SMC has been discovered almost two decades ago and its existence is experimentally well established, little is known about the nature of the responsible interaction. This means in particular, that the functional form of $s(h)$, that is the exact dependence of the interaction strength on the distance between substrate and monolayer, is not known. Nevertheless, it has been possible to estimate at least its overall strength by measuring the pressure difference, $\Delta\pi$, between the co-existence pressures of a monolayer floating in the trough and at the substrate. It turned out that the coexistence pressure is lowered by roughly 40% due to SMC.[42] However, many details of the interaction are still unknown and remain to be investigated either by further experiments or by a microscopic theory. One can nevertheless impose a set of minimal constraints on the function $s(h)$. Since SMC facilitates condensation at the substrate, it necessarily approaches a finite negative value for vanishing h. In addition, s must quickly approach zero for increasing film height, h, since SMC is never observed to occur on water films more than a few nanometers thick. By these conditions, one can at least limit the choice of $s(h)$ to a certain class of functions. Of course, for any numerical calculation, one has to provide an explicit expression for the height dependence. Throughout this article, we will always assume that SMC acts on the same lengthscale as the substrate–water interaction. This means that we choose $s(h) = b\Psi(h)$, where Ψ is the potential of the disjoining pressure characterizing the substrate–water interaction as will be explained in detail in the next section.

3.2. Model of the Transfer Process

In order to model the transfer process, we consider a solid substrate that is withdrawn in the negative x-direction from a water reservoir with a constant velocity v. We focus on the region close to the contact line (see Figure 6).

The moving substrate carries a film of water from the reservoir and the balance of this water supply and evaporation of the film yields the formation of a meniscus. The water bath is assumed to be covered with a homogeneous LE surfactant layer, which flows with the water towards the contact line. The water film in the considered region is sufficiently thin to be amenable to the lubrication approximation, an approximation of the basic equations of fluid flow, the Navier–Stokes equations, for thin-film problems. This approximation has a long history and has first been applied by Reynolds.[46] The term "lubrication approximation" stems from the fact that,

NANO MICRO small

although it is nowadays successfully applied to describe thin liquid films with free surfaces,[47,48] it was originally invented to model liquids in a narrow space between two plates.

Within the framework of the approximation, the water film is described by its height profile $h(\vec{x}, t)$ that indicates the film thickness above a point $\vec{x}$ on the substrate. The surfactant layer at the surface of the film can described by a continuity equation of the form $\partial_t \Gamma = -\nabla(\Gamma \tilde{\vec{u}})$ where $\tilde{\vec{u}}$ denotes the flow velocity at the surface of the water. Thus the time evolution of the surfactant is directly dependent on the flow in the water film. Conversely, γ affects the water flow via the surface tension that is related to the surface pressure by $\sigma = \sigma_0 - \pi$. The value of π is determined by the local surfactant density and its gradients as has been explained in the previous section. After a suitable set of scales h_0, l_0, t_0, γ_0, and σ_0 for height, length, time, surfactant density, and surface tension, respectively, has been introduced, the time evolution equations for the nondimensionalized height profile $H(\vec{X}, T) := h(\vec{X}l_0, Tt_0)/h_0$ and the surfactant density $\Gamma(\vec{X}, T) := \gamma(\vec{X}l_0, Tt_0)/\gamma_0$ take the explicit form

$$\partial_T H = -\nabla\left(\frac{-H^3}{3}\nabla\overline{P} + \frac{H^2}{2}\nabla\hat{\Sigma} - V\vec{e}_X H\right) - E_{ev}\delta\mu \qquad (3)$$

$$\partial_T \Gamma = -\nabla\left(\frac{-\Gamma H^2}{2}\nabla\overline{P} + \Gamma H\nabla\hat{\Sigma} - V\vec{e}_X\Gamma\right) \qquad (4)$$

In these equations, the generalized pressure $\bar{P} = -(1 - \varepsilon^2\Pi_{\text{hom}}(\Gamma))\nabla^2 + \Phi(H)$ takes both the Laplace pressure as well as the nondimensionalized disjoining pressure Φ into account. The former links the curvature of the water surface to the pressure difference between liquid and air while the latter describes the wetting properties of the substrate. The disjoining pressure was experimentally discovered by Derjaguin and co-workers in the thirties of the last century.[49] Although it is clear, that Φ depends on the thickness of the liquid film, several possible forms of this dependence are discussed in the literature.[47,50] The most common choices are of the form

$$\phi(h) = \frac{a_3}{h^3} - \frac{a_n}{h^n} \qquad (5)$$

with $n \in N$, $n > 3$ and $a_3, a_n > 0$. The term $\propto h^{-n}$ originates from the van-der-Waals forces acting between the surfaces of the substrate and the liquid–vapor interface of the film (see chapter 13 of Israelachvili[51]) and describes, in the case of Equation 5, a long-range attraction. The constant a_3 is related to the Hamaker constant A,[52] which is commonly used to quantify van-der-Waals interactions, by $a_3 = -A/(6\pi)$. The term $\propto h^{-n}$ describes a shortrange repulsive interaction. Due to this interaction, the substrate does not dry to $h = 0$ but is always covered with a precursor film whose height h_p is determined by the equation $\phi(h_p) = 0$. Thus, Equation 5 describes a partial wetting substrate with a precursor of height h_p. More details on the properties of the precursor film can be found in the reviews by de Gennes and by Bonn et al.[53,54] The value of n could not be determined by experiments, so far.[55] In the following, the choice $n = 6$, that has been discussed by Pismen and Eggers,[55–57] is adopted. The precursor height is the an intrinsic height scale of the system so that it is convenient to choose $h_0 = h_p$, so that $H_p = 1$. The characteristic lenght and time scales of the system are defined by $l_0 = \gamma_0\sqrt[3]{\kappa/\sigma_0}$ and $t_0 = \gamma_0^4\kappa^2\eta/(h_0^3\sigma_0^3)$, respectively. Furthermore, we choose $\gamma_0 = \gamma_{\text{cr}}$ and $\sigma_0 = \sigma_w - \pi_{\text{hom}}(\gamma_{\text{cr}})$. Then the dimensionless parameter $\varepsilon = \sqrt[3]{\sigma_0/(\gamma_0\kappa)}(a_6/a_3)^{1/3}$ relates the forces acting at the monolayer covered surfaces, characterized by σ_0, γ_0 and κ, to the wetting interaction described by a_3 and a_6.[40] Spatial variations of the monolayer density lead to gradients of surface tension that induce Marangoni forces. These are included in the model by the terms involving $\nabla\hat{\Sigma} = -\nabla\Pi_{\text{hom}}(\Gamma) + \varepsilon^{-2}\Gamma\nabla^3\Gamma$. Here, $\Pi_{\text{hom}}(\Gamma)$ is the nondimensionalized surface pressure of a homogeneous surfactant layer of density Γ. Furthermore, both Equation 3 and 4 contain an advective term proportional to the transfer velocity $V\vec{e}_X$ with the dimensionless transfer velocity $V = vt_0/l_0$ and the unit vector in X-direction $\vec{e}_X$, to describe how water and surfactants are dragged by the moving substrate. Evaporation of the water film leads to the presence of a non-mass-conserving contribution $E_{ev}\delta\mu$ to Equation 3. Here $\delta\mu = \mu_w - \mu_v$ is the difference of the chemical potentials of the water and the vapor phase where as $E_{ev} = \eta l_0^2 Q_e/h_0^3$ is the evaporation number with the effective rate constant Q_e. As the pressure in the vapor is assumed to be close to the saturation pressure, the chemical potential of the water film can be identified with the generalized pressure, that is, $\mu_w = \bar{P}$ and $\mu_v = const.$[58,59]

At this point, it might be objected that the model presented here does not take the elastic properties of the surfactant monolayer into account. However, this approach is valid, as one can estimate the influence of the surface rigidity for DPPC in the LE and LC phases to be neglectable compared to the influence of the tension of a clean water surface.[40] In order to model the transfer of layers with higher rigidity it is necessary to extend the above model by inclusion of the corresponding Helfrich energy of a stiff interface.[60] This yields the presence of an additional term $\propto\nabla^6 H$, increasing the order of the considered equations by two.[61]

3.3. Transfer onto Solid Substrates

In order to model transfer of a floating LE monolayer onto a substrate, we employ the boundary conditions $\Gamma(L) = \Gamma_L$, $\partial_X^2\Gamma(L) = \partial_X\Gamma(0) = \partial_x^2\Gamma(0)$, $H(L) = H_L$, $\partial_X^2 H(L) = \partial_X H(0) = \partial_X^2 H(0)$ in X-directions as well as periodic boundary conditions in Y-direction. Here, the constant boundary values H_L and Γ_L correspond to the film height and the monolayer density of the reservoir which is set to the value corresponding to the LE phase. Numerical solution of the Equation 3 and 4 subject to these conditions shows the existence of a certain range of transfer velocities (V_l, V_u), subsequently called the *patterning range*, for which regular stripe patterns are obtained.[40,62] One can distinguish two main transfer modes within the patterning range: for lower velocities, stripes perpendicular to the contact line are observed, while stripes parallel to the contact line are generated for higher V. Interestingly, the perpendicular stripes occur after a transient period during which a number of stripes parallel to the contact line is formed (see **Figure 7**).

The details of the observed stripe patterns depend on the transfer velocity. For the case of stripes parallel to the contact line, this dependence can be studied by use of 1D calculations.

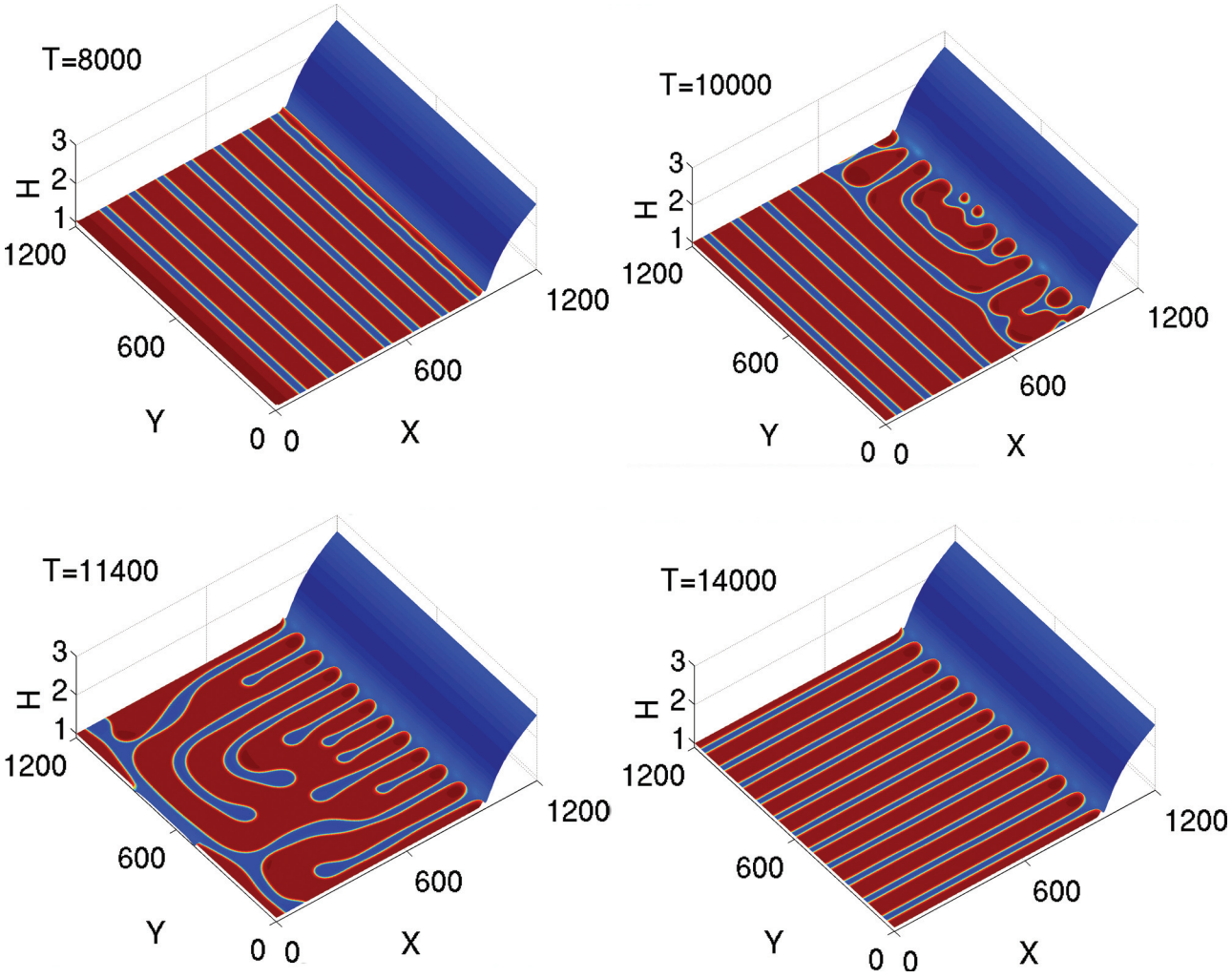

Figure 7. In 2D simulations, a transition between stripes parallel to the contact line and stripes perpendicular to the contact line is observed at a transfer velocity $V = 0.44$. More images and information about the transfer onto homogeneous substrates can be found in Köpf et al.[62]

Figure 8 shows snapshots from time simulations of 1D solutions at various values of V. Clearly, the wavenumber of the observed stripe patterns changes significantly with the pull velocity. This is summarized in **Figure 9** that shows the wavenumber k of the pattern as a function of V. This numerically obtained curve can be compared to similar diagrams obtained from experiments.[19,20,24,27,63] The qualitative agreement with the experimental data is striking: For low velocities, patterns with very large periods are observed. The minimal spatial periodicity is achieved for an intermediate V. At the high velocity end of the patterning range, the periodicity increases again and finally, the range ends abruptly. As the model calculations correctly predict, the formation of stripes perpendicular to the contact line are observed for low velocities, close to the left boundary of the patterning range. Chen et al. present a phase diagram showing which patterns are obtained for several different values of the surface pressure and the transfer velocity.[20] Clearly, it is difficult to achieve quantitative agreement. This difficulty stems from the fact that the calculation involves a number of material parameters that are not known exactly from the experiments such as the exact form of the disjoining pressure and most importantly the distance dependence of the substrate-mediated condensation effect, that is, the SMC function $s(h)$ in Equation 2. Nevertheless, the theory is able to reproduce the qualitative behavior of the experimental system and it can be applied to predict the response to changes of other parameters besides the pull velocity V. One such parameter is the temperature τ of the water subphase. Its effect on the solutions of the Equation 3 and 4 will be discussed in the following section. Furthermore, first steps to predict pattern formation for the case of a prepatterned substrate have been performed.[40] It has been shown that nonlinear resonance effects may lead to modulated stripe patterns.

3.4. The Impact of Temperature

Since the pattern formation is directly connected to the thermodynamics of the surfactant monolayer, temperature is an important control parameter. In particular, a change of the temperature τ yields a shift of the surface pressure isotherm,

small NANO MICRO

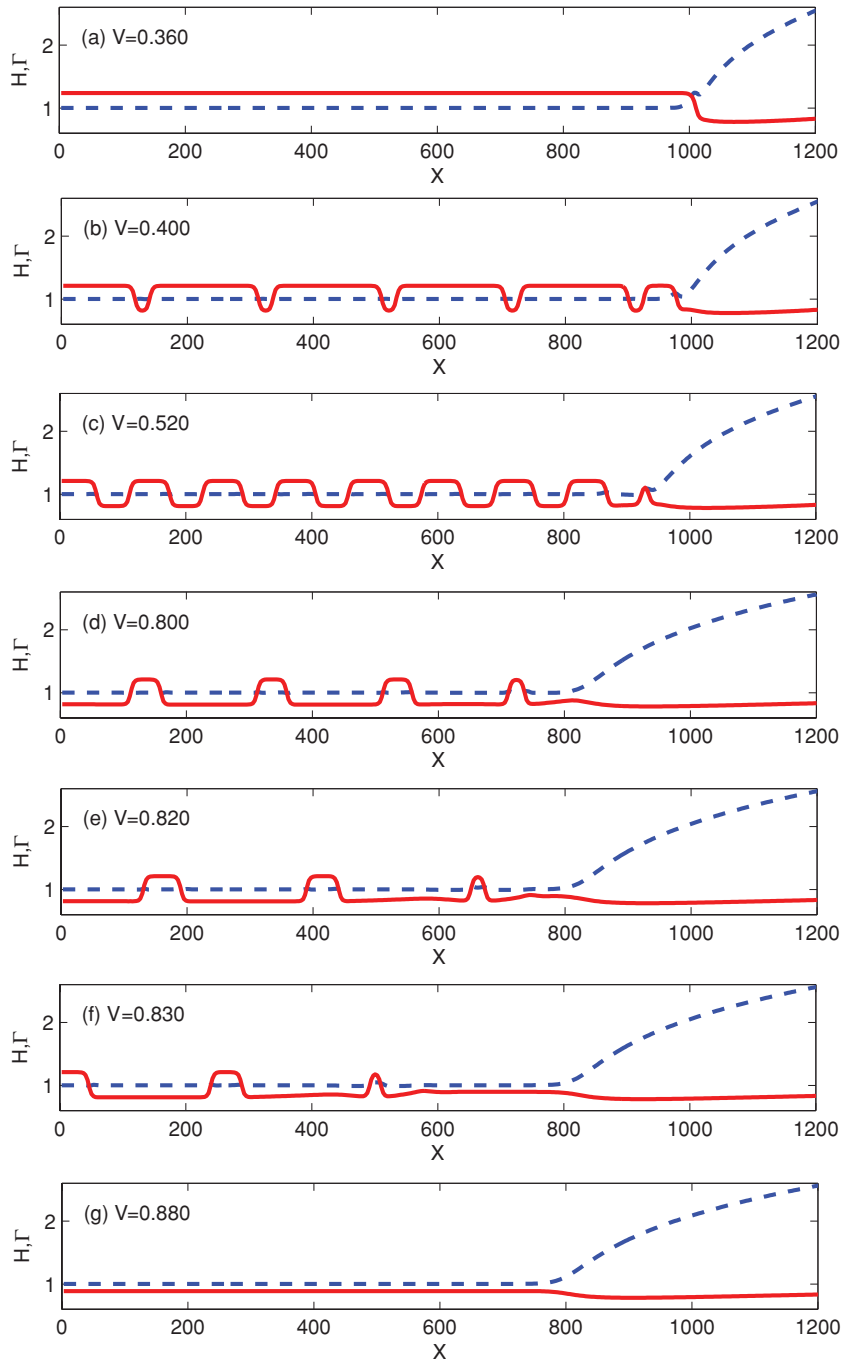

Figure 8. Snapshots from 1D computations of monolayer transfer with seven different velocities. The solid red line is the density of the monolayer Γ wheras the dashed blue line is the height profile H of the water film. The letters (a to g) correspond to the labels in Figure 9.

so that the function π_{hom} in Equation 1 has to be considered as a function of the surfactant density γ and the subphase temperature τ. Systematic experimental measurements and numerical simulations at different temperatures show that the patterning range is shifted towards lower transfer velocities and becomes smaller and smaller as the temperature increases.[64] This is intuitively understandable because the patterning range eventually has to disappear at the critical temperature τ_{cr} of the LE-LC phase transition above which the two phases are no longer distinguishable. **Figure 10** shows the wavenumber $k(V)$ of stripe patterns as a function of the transfer velocity that is obtained from numerical simulation for four different temperatures between 20 and 27 °C. Clearly changes of the subphase temperature of only a few Kelvin change the periodicity significantly. For the most velocities, the wavenumber decreases with increasing temperature (see for example the intersections of $k(V)$ with the vertical line at $V = 0.54$ in Figure 10). Furthermore, it is possible to switch from homogeneous LC transfer to stripe patterns and finally to homogeneous LE transfer by adjusting only the temperature τ at constant pulling velocity V. This is the case, e.g., for $V = 0.45$ (see corresponding vertical line in Figure 10) which lies below the patterning range for $\tau = 20$ °C, within the range for $\tau =$ 22 and 25 °C, and above the range for $\tau =$ 27 °C. Thus, the knowledge of the temperature dependence allows for an enhanced controllability of structures produced by LB patterning.

4. Transfer-Induced Pattern Formation of Other Materials

The controllable assembly of nanoparticles and functional organic/biomaterials has received increased attention in the last decade. Some of these materials can be patterned by means of the LB technique in a direct transfer manner similar to DPPC patterning. Dip-coating, another typical dynamic self-assembly process, is one of the well-known wet coating techniques to prepare large-area and uniform coating on a substrate. In some cases, various patterns can spontaneously form on energetically and topologically homogeneous surfaces during dip-coating process under optimized conditions.

4.1. LB Patterning of Nanoparticles

There has been progress reported on the close-packed monolayer fabrication of ligand-stabilized nanomaterials on solid substrate,[65–67] since the appealing feature of the LB technique is the intrinsic control of the internal layer structure down to a molecular level and the precise control of the resulting film thickness. Unlike these traditional close-packed nanoparticle monolayers on solid substrates, the LB technique itself also is a way to obtain regular nanoparticle or nanowire pattern arrays on a solid substrate.[68]

Contrary to the normal method for LB assembly of nanoparticles, where higher-order nanoparticle structures are

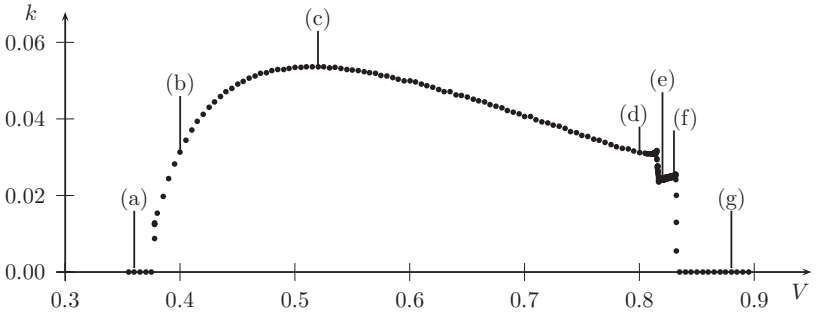

Figure 9. The wavenumber *k* of patterns transferred onto homogeneous substrates against the pull velocity *V* as obtained from 1D computations. The curve is non-monotonous, so that the same wavenumber *k* can be obtained for high and low values of *V*.

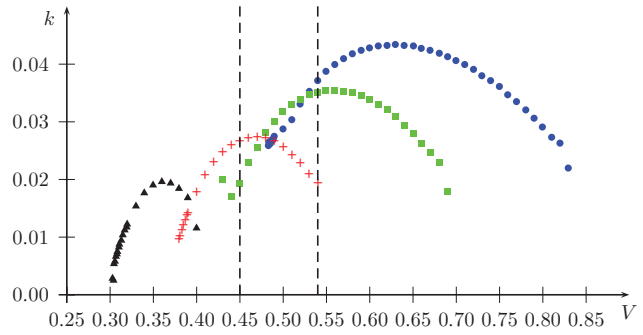

Figure 10. The wavenumber *k* as a function of the transfer velocity *V* for four different temperatures: $\tau = 20$ °C (blue circles), $\tau = 22$ °C (green squares), $\tau = 25$ °C (red crosses), and $\tau = 27$ °C (black triangles).

formed at the air–water interface before they are transferred onto a solid substrate, Schmid and Yang et al. found that the process of LB transfer is also an efficient way to obtain regular nanoparticle arrays on solid substrates with the help of dewetting during the LB transfer process.[29–31,65–69] As first reported, Schmid et al.[69] successfully obtained parallel rows of $Au_{55}(PPh_3)_{12}Cl_6$ clusters, quasi-1D structures of quantum dots of about 10 nm in width, using the LB technique. A modified LB technique (**Figure 11**) with a deposition angle of 20° was used to generate this kind of cluster stripes. The pattern formation is mainly dependent on the speed at which the substrate is moved. At speeds of ~10 cm min^{-1}, the parallel stripes consisting of 3–4 cluster rows with a separation of 8 nm from each other, as shown in Figure 11. The formation of such patterns was attributed to the existence of water meniscus oscillation at the substrate, inducing the generation of stripe patterns running parallel to the meniscus.

Yang et al.[30] used the LB technique to generate well-spaced, parallel, single-particle lines on a substrate from a dilute Langmuir particle monolayer via a stick-slip motion of the water–substrate contact line. They could observe in situ a stick-slip motion of the three-phase contact line during the transfer process by optical microscopy, which is due to the large interline distance and low density of Langmuir monolayer at the air–water interface compared with the work from Schmid et al.[69] The particle density within the lines is controllable by the particle concentration in the monolayer as well as the pulling speed of the substrate. Lines of a great variety of materials and sizes, ranging from a few nanometers to a few micrometers, have been demonstrated as shown in **Figure 12**. The ability of assembling nanoparticles into 1D array enables the construction of higher hierarchical device structures. For example, using gold nanoparticle seeds, vertical single nanowire arrays of silicon can be grown, replicating the pattern of the single particle lines. The spontaneous formation of ordered gold and silver nanoparticle stripe patterns was also found through dewetting a dilute film of polymer-coated nanoparticles on the water surface.[29] Intriguingly, the nanoparticle stripe patterns are perpendicular to the air–water interface, contrary to the above two examples. For this system, the vertical nanoparticle stripe pattern forms due to the fingering instability. These samples have shown that LB technique opens up a new avenue for lithography-free patterning of nanoparticle arrays for various applications including multiplexed surface-enhanced Raman substrates and templated fabrication of higher-order nanostructures.

4.2 Patterning of Other Functional Molecules

Pattern formation by substrate-induced condensation during LB transfer or the stick-slip effect as described above should be a general phenomenon, which is also observed by other

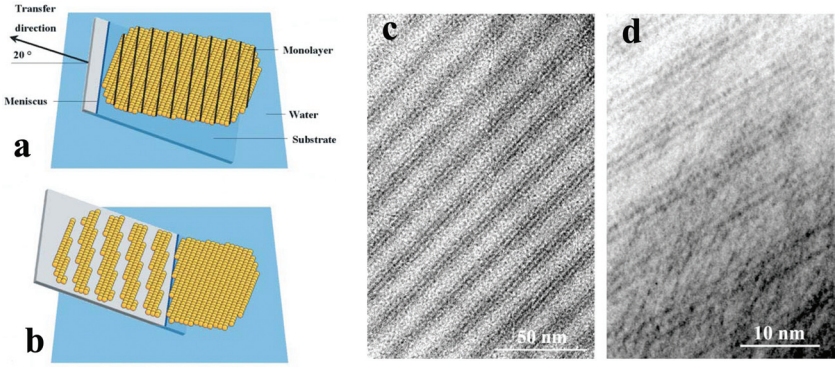

Figure 11. a) Sketch of the formation of cluster stripes from an ordered monolayer. The monolayer is oriented toward the substrate edge and the meniscus, respectively, by a non-predetermined angle. b) Owing to the movement of the substrate from the water and the herewith-linked transfer of the monolayer onto the substrate surface, the monolayer is fractured along the black lines due to the oscillation of the meniscus. Stripes of 3–4 rows of clusters lying side by side are formed. The stripes run parallel to the water meniscus. c) Transmission electron microscopy (TEM) image of cluster stripes consisting of 3–4 cluster rows. d) Magnified cut-out. The cluster rows consist of equidistantly ordered clusters. Reprinted with permission.[69] Copyright 2001, American Chemical Society.

small NANO MICRO

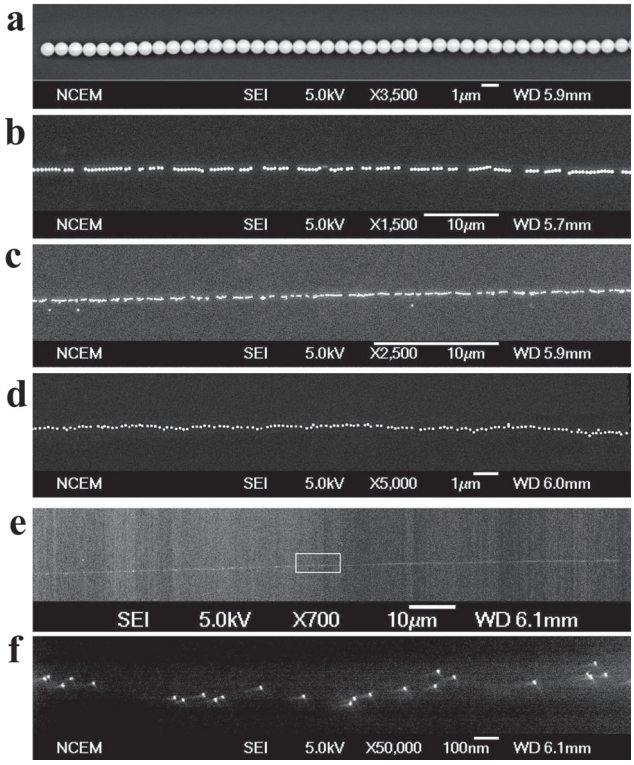

Figure 12. Results of 1D arrays of colloidal particles with a wide range of sizes and materials. A couple of examples are shown in the scanning electron microscopy (SEM) images: a) 0.9 μm, b) 450 nm, and c) 160 nm SiO_2 spheres, d) 50 nm Ag nanocubes, and e,f) 7 nm Pt nanoparticles. Panel f is a higher-magnification image showing the details of the Pt line in panel e. Reprinted with permission.[68] Copyright 2008, American Chemical Society.

molecules such as L-α-dimyristoylphosphatidylcholine (DMPC)[22] and (DPPE).[70] However, the experimental window (e.g., subphase water temperature ranging normally within 10–40 °C for LB preparation) limits applying this method directly to many other materials; not all (amphiphilic) molecules will stay in a homogenous distributed state in such a temperature range at the air–water interface. Instead of the direct patterning of other materials by searching for optimal conditions, preparing a two-component system is likely to be an effective way to pattern different molecules. DPPC will be taken as one component, the other one can be varied. For instance, 4-(dicyanomethylene)-2-methyl-6-(4-dimethylaminostyryl)-4H-pyran (DCM), a typical dye for laser application, and 2-(12-(7-nitrobenz-2-oxa-1,3-diazol-4-yl)-amino)dodecanoyl-1-hexadecanoyl-*sn*-glycero-3-phosphocholine (NBD), a typical dye for bio-labeling, can be used to generate regular and tunable luminescent stripes with submicrometer scale lateral dimensions (**Figure 13**).[71] The dye molecules are uniformly distributed within the expanded DPPC channels, which are separated by condensed DPPC stripes. The width and periodicity of the luminescent stripes can be controlled by adjusting the ratio of dye to DPPC, as shown in Figure 13c. It is worth mentioning that some of the dye molecules used (DCM, Nile red, and oligo(*p*-phenylenevinylene)) are non-amphiphilic water-insoluble molecules, suggesting that this method can also be employed for patterning other water-insoluble materials.

Recently, the same concept was applied to pattern radical initiators. In a mixed monolayer consisted of DPPC and the radical initiator, the radical initiator could be arranged in the channel regions by LB transfer. Subsequently followed by surface initiated polymerization (SIP), regular stripes of polystyrene and polyacrylate brushes were obtained, as schematically depicted in **Figure 14**.[72] The polymer stripe width can be adjusted ranging from about 0.2 to 1.3 μm with the height of the brush polymer reaching 10 nm. Since a reactive group is chosen for covalent attachment of the polymer initiator onto the surface (e.g., silane group to Si wafer), and the group exposed to air can be well designed, this simple and reliable method can be used to create stable, functional, and nanostructured patterns over large areas.

The stripe formation during LB transfer may not necessarily be based on the surface-induced condensation. Rather, the key point is creating meniscus instability. The meniscus oscillations based on a variation of the local subphase composition—rather than surface induced condensation—within the deposited fatty acid monolayer was reported by Vollhardt

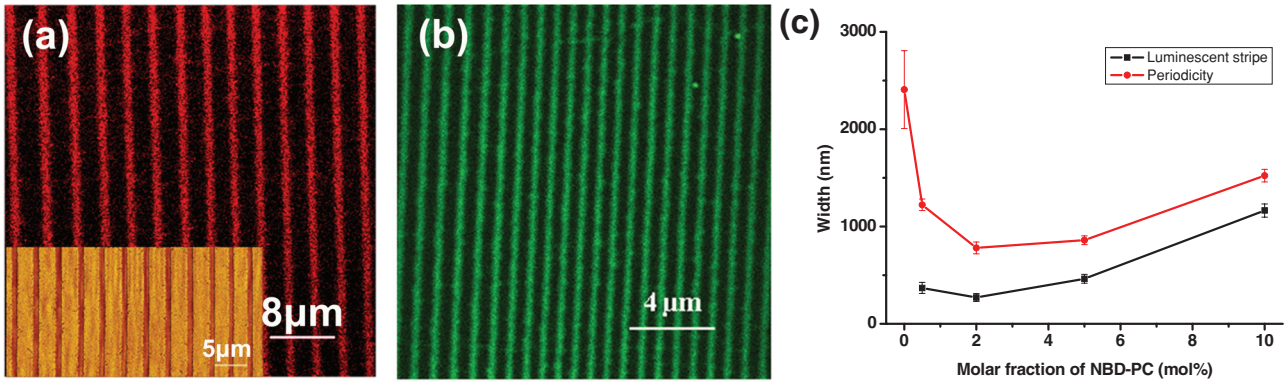

Figure 13. a) Confocal laser scanning microscope (CLSM) image of the regular luminescent stripes formed by DCM/DPPC (5 mol%) at 1.0 mN/m and 10 mm/min. (Excited at 488 nm and detected at 580–700 nm). The inset in the CLSM image shows an AFM image of the stripe pattern. b) CLSM images of mixed monolayers of NBD/DPPC (2 mol%) at 2.0 mN/m and 20 mm/min. (Excited at 488 nm and detected at 500–600 nm). c) Dependence of the luminescent stripe width and periodicity on the molar fraction of NBD. Reprinted with permission.[81] Copyright 2007, American Chemical Society.

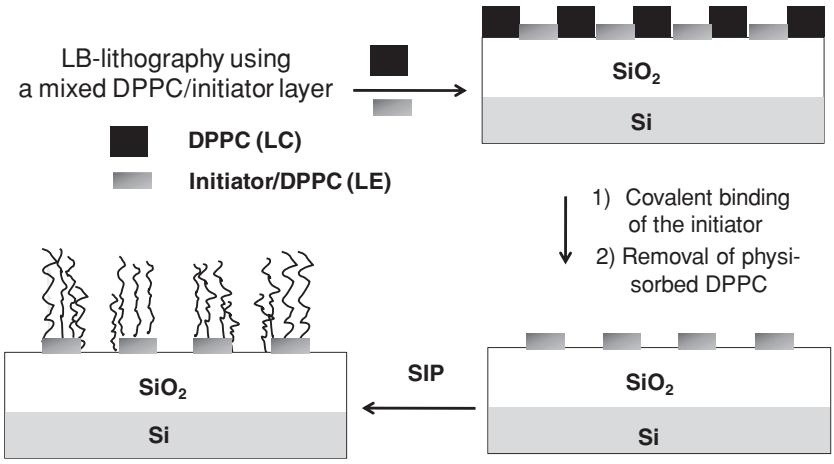

Figure 14. Concept of fabrication patterned polymer brushes by patterning the polymer initiators. LC = liquid condensed phase, LE = liquid expanded phase Reprinted.[71]

and co-workers.[36] In their case, counter metal ions were used in the water subphase. In considering the LB deposition process, one should take into account that a deposited monolayer can contain only the neutral molecules of fatty acid or of the corresponding salt. The motion of a charged surface relative to the bulk solution will always accompany concentration polarization. For the case of monolayer deposition, the concentration polarization effect can be sufficient to produce a significant local change of the subphase composition, thus induce the meniscus stability, overlapping with complicated hydrodynamic processes. In other studies, stripe pattern formation in a mixed monolayer of DPPC with a lipopolymer or with 1,2-dilaurolyl-*sn*-glycero-3-phosphocholine (DLPC) were reported by Purrucker et al.[31] and Moraille et al.[73] Both systems are transferred at a relatively higher surface pressure regime. The stripes in the former case are perpendicular to the three-phase contact line, whereas in the latter case they are parallel to the three-phase contact line. In both cases, the mechanisms are not based on the surface-induced condensation but on wettability-induced phase separation (former case) and shear force-induced alignment/distortion of DPPC solid domains in the DLPC fluid matrix, as proposed by the authors.

4.3. Dentrite Pattern Formation by Dip-Coating

Besides LB transfer process, dip-coating is another attractive method to prepare various patterns.[74–80] There are some common and different features between these two techniques: 1) Regarding the pattern formation, LB and dip-coating techniques are based on the similar concepts in some cases including contact line deposition, finger instability effect, and/or stick-slip behavior. 2) LB requires the transfer of materials from a volatile organic solvent to a water surface; therefore, materials should be compatible with both organic solvent and water, whereas diverse systems such as homogeneous solutions and heterogeneous suspensions can be used in dip-coating process. 3) LB has a unique ability to precisely produce monolayer patterns because, in principle, only monolayer or submonolayer was transferred onto substrate. Dip-coating can prepare various patterns with thickness control since the deposition quantity can be well tuned in different ways, for example by changing the concentration of solution and suspension, pulling speed, or spatial condition of evaporation. In addition, the capillary flow at the meniscus can carry the solutes or dispersed materials forward to the contact line where the deposition occurs, which also provides a way to control deposition quantity compared with LB method.

Patterning dispersible nanoparticles and nanowires and soluble chemicals by dip-coating has been documented in literature. Generally, regular stripes, 1D nanoparticle array, and 2D nanowire array with orientation perpendicular or parallel to the contact line have been achieved in different systems. In this section, we will give a brief summary of previous work, and focus on a special growth of dendrite patterns with thickness control with monolayer precision via dip-coating process.

Inspired by the "coffee ring stain" effect, Yang et al.[74] utilized dip-coating technique to produce nanowire arrays over large area from nanowire dispersion-the most common form of nanowire stocks. In their work, selective positioning of Ag nanowire arrays with controllable alignment, spacing, and density was achieved based on the concept of the stick-slip motion of the contact line during dip-coating. Stebe et al.[75] reported that withdrawal of a plate from an aqueous particle suspension yielded periodic horizontal stripes. Depending on the withdrawal velocity relative to transition velocity at which a thin film of liquid is entrained above the meniscus, the stripe patterns with tunable width, spacing, and thickness were fabricated. Pei et al.[78] demonstrated the in situ growth and patterning of aligned organic semiconductor nanowire arrays from homogeneous solution via dip-coating. By optimizing stick-slip motion, the spatial condition for solvent evaporation, and the solution concentration, parallel organic nanowire arrays with controllable length, density, and periodicity were directly grown and aligned on the substrates.

As described above, dip-coating generally produce patterns in stripe or array with orientation perpendicular or parallel to the contact line. The thickness control in conventional dip-coating system is about tens of nm or even more. Recently, we reported the growth of dendrite patterns of an organic semiconductor (DTBDT-C9, **Figure 15**a) with thickness control with monolayer precision.[80] During the dip-coating process, the withdrawal velocity (U) was systematically adjusted, which appeared to have a great influence on the growth of the molecules, mainly on the fractal morphology of microstripes (Figure 15c–f) as well as on the number of molecular layers (N) of microstripes (**Figure 16**a). As shown in Figure 15c–f, withdrawal of substrate from DTBDT-C9 solution at different velocity generally yields partially aligned dendrite patterns, but the precise structure of these patterns exhibits obvious dependence on the withdrawal

small NANO MICRO

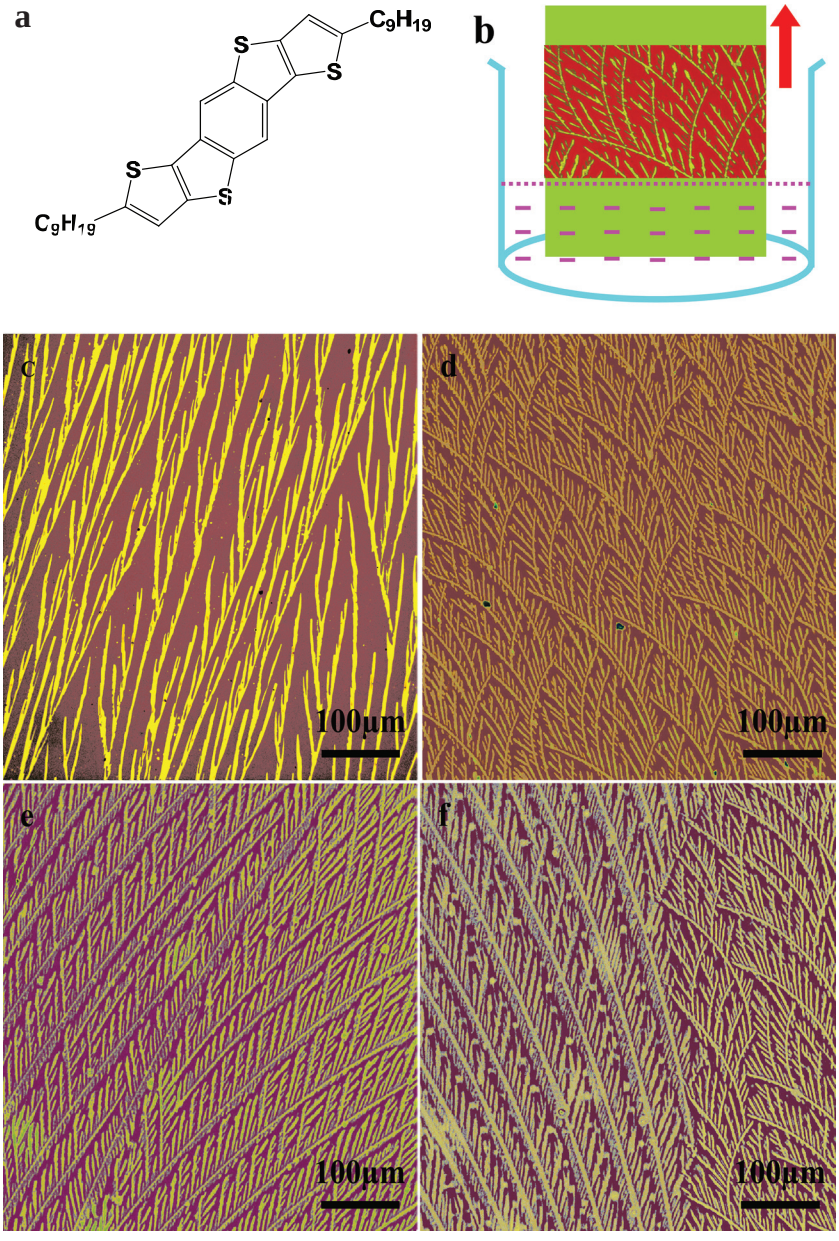

Figure 15. a) Molecular structure of DTBDT-C9. b) Schematic diagram of dip-coating process. Optical images of large-area stripes of c) mixed multilayer, d) pure bilayer, e) pure monolayer, and f) cross-area between bilayers (right) and monolayers (left). Reprinted with permission.[80] Copyright 2010, American Chemical Society.

velocity or the number of molecular layers of microstrips. This feature is clearly different from the characteristics of patterns described above. Figure 16a reveals that the number of molecular layers decreases with the increasing withdrawal velocity. Lower withdrawal velocity yields mixed multilayers (3–9 monolayers). It is noteworthy that pure monolayer and bilayer microstripes over large areas (Figure 16b,c) can be obtained at high withdrawal velocity. Under optimized conditions, pure trilayer and tetralayer dentrite patterns over large area have been obtained as well. The controllable growth of dentrite microstripe patterns with monolayer precison provides a powerful system for fundamental research and device applications.

5. Conclusion and Outlook

We have reviewed recent experimental and theoretical work on the fabrication of well-ordered mesoscopic structural surfaces over large areas by the LB and dip-coating techniques. Theoretical progress has led to a rather complete description of the dynamical self-organization processes underlying LB patterning. The experimental results summarized here show that dynamic self-assembly may be able to successfully control and modify the surface patterning, which is a prerequisite if LB patterning[81] is to become a candidate for the assembly of nanostructures into integrated device architectures.[82–85] The wider use of different materials opens the possibility of extending the methods to other pattern-generating chemical systems. The mesoscopic structural surfaces described here may serve as a platform for engineering biological–material interfaces, for instance, surfaces for controlled cell adhesion and specific interactions with biocomponents. Moreover, in combination with biomaterials (protein, DNA, polysaccharide), mesoscopically structured surfaces may contribute to construction of biofunctionalized structures and "programmed" systems.

Acknowledgements

We thank the previous and present group members, especially M. Gleiche, X. D. Chen, N. Lu, S. Lenhert, M. Hirtz, M. Zhang, J. Y. Hao, Y. Li, and X. Wu, for contributing to the work summarized herein. We acknowledge the fruitful collaboration with G. Schmid, A. L. Rogach, M. Wang, Y. Wang, L. Wu, and A. Studer. We thank the DFG for financial support (German-Chinese Transregional collaborative Research Center TRR61).

This Review is part of the Special Issue on Multilevel Molecular Assemblies: Structure, Dynamics, and Functions, featuring contributions from the Transregional Collaborative Research Center (TRR 61).

[1] W. Menz, J. Mohr, O. Paul, *Microsystem Technology*, 2nd ed., Wiley-VCH, Weinheim, Germany **2001**.
[2] N. L. Rosi, C. A. Mirkin, *Chem. Rev.* **2005**, *105*, 1547.
[3] P. Ball, *The Self-Made Tapestry: Pattern Formation in Nature*, Oxford University Press, Oxford **1999**.
[4] B. D. Gates, Q. B. Xu, M. Stewart, D. Ryan, C. G. Willson, G. M. Whitesides, *Chem. Rev.* **2005**, *105*, 1171.
[5] T. Ito, S. Okazaki, *Nature* **2000**, *406*, 1027.

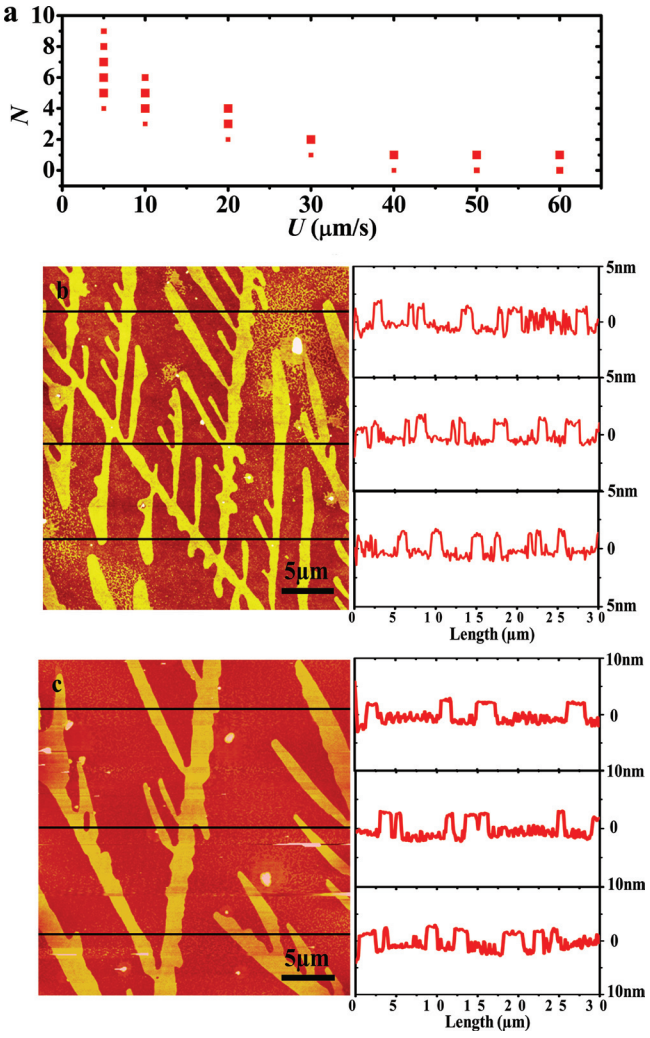

Figure 16. a) The evolution of the number of molecular layers (*N*) with withdrawal velocity (*U*). The size of the symbol represents the schematic (not real) distribution of each layer at a given velocity. 0 layer denotes a discontinuous island. AFM image and section analysis of b) monolayer and c) bilayer microstripes. Reprinted with permission.[80] Copyright 2010, American Chemical Society.

[6] M. Geissler, Y. N. Xia, *Adv. Mater.* **2004**, *16*, 1249.
[7] G. M. Whitesides, B. Grzybowski, *Science* **2002**, *295*, 2418.
[8] L. G. Gains, *Insoluble Monolayers at Liquid-Gas Interfaces*, Interscience Publishers, New York **1969**.
[9] H. Kuhn, D. Mobius, *Investigation of Surface and Interfaces - Part B*, *Physical Methods of Chemistry Series* (Eds: W. R. Bryant, C. B. Roger), John Wiley & Sons, Inc., New York **1993**; Vol. IXB.
[10] G. Roberts, *L. angmuir-Blodgett Films,* Plenum Press, New York **1990**.
[11] X. D. Chen, J. B. Wang, N. Shen,Y. H. Luo, L. Li, M. H. Liu, R. K. Thomas, *Langmuir* **2002**, *18*, 6222.
[12] X. D. Chen, J. B. Wang, M. H. Liu, *J. Colloid Interface. Sci.* **2005**, *287*, 185.
[13] X. Huang, C. Li, S. G. Jiang, X. S. Wang, B. W. Zhang, M. H. Liu, *J. Am. Chem. Soc.* **2004**, *126*, 1322.
[14] L. Zhang, N. Gaponik, J. Muller, U. Plate, H. Weller, G. Erker, H. Fuchs, A. L. Rogach, L. F. Chi, *Small* **2005**, *1*, 524.
[15] H. M. McConnell, *Ann Rev. Phy. Chem.* **1991**, *42*, 171.
[16] H. Möhwald, *Ann. Rev. Phy. Chem.* **1990**, *41*, 441.
[17] H. Riegler, K. Spratte, *Thin Solid Films* **1992**, *210*, 9.
[18] K. Spratte, L. F. Chi, H. Riegler, *Europhys. Lett.* **1994**, *25*, 211–217.
[19] M. Gleiche, L. F. Chi, H. Fuchs, *Nature* **2000**, *403*, 173.
[20] X. D. Chen, N. Lu, H. Zhang, M. Hirtz, L. X. Wu, H. Fuchs, L. F. Chi, *J. Phy. Chem. B* **2006**, *110*, 8039.
[21] S. Lenhert, L. Zhang, J. Mueller, H. P. Wiesmann, G. Erker, H. Fuchs, L. F. Chi, *Adv. Mater.* **2004**, *16*, 619.
[22] A. Raudino, B. Pignataro, *J. Phys. Chem. B* **2007**, *111*, 9189.
[23] N. Lu, M. Gleiche, J. W. Zheng, S. Lenhert, B. Xu, L. F. Chi, H. Fuchs, *Adv. Mater.* **2002**, *14*, 1812.
[24] M. Hirtz, H. Fuchs, L. F. Chi, *J. Phys. Chem. B* **2008**, *112*, 824.
[25] J. G. Petrov, B. P. Radoev, *Colloid Polym. Sci.* **1981**, *259*, 753.
[26] J. Yuan, T. M. Fischer, *Langmuir* **2007**, *23*, 3603.
[27] S. Lenhert, M. Gleiche, H. Fuchs, L. F. Chi, *ChemPhysChem* **2005**, *6*, 2495.
[28] X. D. Chen, M. Hirtz, H. Fuchs, L. F. Chi, *Langmuir* **2007**, *23*, 2280.
[29] J. X. Huang, T. Kim, A. R. Tao, S. Connor, P. D. Yang, *Nat. Mater.* **2005**, *4*, 896.
[30] J. X. Huang, A. R. Tao, S. Connor, R. R. He, P. D. Yang, *Nano Lett.* **2006**, *6*, 524.
[31] O. Purrucker, A. Fortig, K. Ludtke, R. Jordan, M. Tanaka, *J. Am. Chem. Soc.* **2005**, *127*, 1258.
[32] J. Mahnke, D. Vollhardt, K. W. Stöckelhuber, K. Meine, H. J. Schulze, *Langmuir* **1999**, *15*, 8220.
[33] M. L. Kurnaz, D. K. Schwartz, *J. Phys. Chem.* **1996**, *100*, 11113.
[34] V. Kovalchuk, D. Vollhardt, *Adv. Colloid Interface. Sci.* **2005**, *114–115*, 267.
[35] V. Kovalchuk, E. Zholkovskiy, M. Bondarenko, V. Starov, D. Vollhardt, *Adv. Colloid Interface Sci.* **2011**, *168*, 114.
[36] V. I. Kovalchuk, M. P. Bondarenko, E. K. Zholkovskiy, A. Vollhardt, *J. Phys. Chem. B* **2003**, *107*, 3486.
[37] A. W. Adamson, *Physical Chemistry of Surfaces*, Wiley Interscience, New York, New York **1990**.
[38] V. Kaganer, H. Möhwald, P. Dutta, *Rev. Mod. Phys.* **1999**, *71*, 779.
[39] M. H. Köpf, S. V. Gurevich, R. Friedrich, *Europhys. Lett.* **2009**, *86*, 66003.
[40] M. H. Köpf, S. V. Gurevich, R. Friedrich, *Phys. Rev. E* **2011**, *83*, 016212.
[41] L. D. Landau, E. M. Lifschitz, *Statistische Physik, Teil 1*, Akademie Verlag, Berlin, East Germany **1987**.
[42] K. Spratte, H. Riegler, *Langmuir* **1994**, *10*, 3161.
[43] K. Graf, H. Riegler, *Colloid Surf. A-Physicochem. Eng. Asp.* **1998**, *131*, 215.
[44] S. Leporatti, F. Bringezu, G. Brezesinski, H. Möhwald, *Langmuir* **1998**, *14*, 7503.
[45] S. Leporatti, G. Brezesinski, H. Möhwald, *Colloid Surf. A-Physicochem. Eng. Asp.* **2000**, *161*, 159.
[46] O. Reynolds, *Phil. Trans. Roy. Soc.* **1886**, *177*, 157.
[47] A. Oron, S. H. Davis, S. G. Bankoff, *Rev. Mod. Phys.* **1997**, *69*, 931.
[48] R. V. Craster, O. K. Matar, *Rev. Mod. Phys.* **2009**, *81*, 1131.
[49] B. V. Derjaguin, *Colloid Polym. Sci.* **1975**, *253*, 492.
[50] U. Thiele, in *Thin Films of Soft Matter* (Eds: S. Kalliadasis, U. Thiele), Springer, Vienna, Austria **2007**, pp. 25–93.
[51] J. N. Israelachvili, *Intermolecular and Surface Forces*, Academic Press, London, UK **2011**
[52] H. Hamaker, *Physica* **1937**, *4*, 1058.
[53] D. Bonn, J. Eggers, J. Indekeu, J. Meunier, E. Rolley, *Rev. Mod. Phys.* **2009**, *81*, 739.
[54] P. G. deGennes, *Rev. Mod. Phys.* **1985**, *57*, 827.
[55] L. M. Pismen, J. Eggers, *Phys. Rev. E* **2008**, *78*, 056304.
[56] L. M. Pismen, *Phys. Rev. E* **2001**, *64*, 021603.
[57] L. M. Pismen, *Phys. Rev. E* **2010**, *81*, 026307.
[58] L. Pismen, *Phys. Rev. E* **2004**, *70*, 021601.
[59] U. Thiele, I. Vancea, A. J. Archer, M. J. Robbins, L. Frastia, A. Stannard, E. Pauliac-Vajour, C. P. Martin, M. O. Blunt, P. J. Moriarty, *J. Phys., Condens. Matter* **2009**, *21*, 264016.

[60] W. Helfrich, *Z. Naturforsch.* **1973**, *28C*, 693.
[61] M. H. Köpf, S. V. Gurevich, T. Wulf, R. Friedrich, *Phys. Rev. E* **2011**, *83*, 040601.
[62] M. H. Köpf, S. V. Gurevich, R. Friedrich, L. F. Chi, *Langmuir* **2010**, *26*, 10444.
[63] X. Chen, S. Lenhert, M. Hirtz, N. Lu, H. Fuchs, L. F. Chi, *Acc. Chem. Res.* **2007**, *40*, 393.
[64] M. H. Köpf, H. Harder, J. Reiche, S. Santer, *Langmuir* **2011**, *27*, 12354.
[65] S. W. Chen, *Langmuir* **2001**, *17*, 2878.
[66] G. Markovich, C. P. Collier, S. E. Henrichs, F. Remacle, R. D. Levine, J. R. Heath, *Chem. Res.* **1999**, *32*, 415.
[67] Y. C. Tian, J. H. Fendler, *Chem. Mater.* **1996**, *8*, 969.
[68] A. R. Tao, J. X. Huang, P. D. Yang, *Acc. Chem. Res.* **2008**, *41*, 1662.
[69] O. Vidoni, T. Reuter, V. Torma, W. Meyer-Zaika, G. Schmid, *J. Mater. Chem.* **2001**, *11*, 3188.
[70] M. Gleiche, *Ph.D. Dissertation*, University of Münster, Germany, **2001**.
[71] X. D. Chen, M. Hirtz, H. Fuchs, L. F. Chi, *Adv. Mater.* **2005**, *17*, 2881.
[72] M. K. Brinks, M. Hirtz, L. F. Chi, H. Fuchs, A. Studer, *Angew. Chem. Int. Edi.* **2007**, *46*, 5231.
[73] P. Moraille, A. Badia, *Langmuir* **2002**, *18*, 4414.
[74] J. X. Huang, R. Fan, S. Connor, P. D. Yang, *Angew. Chem. Int. Edit.* **2007**, *46*, 2414.
[75] M. Ghosh, F. Q. Fan, K. J. Stebe, *Langmuir* **2007**, *23*, 2180.
[76] O. Giraldo, J. P. Durand, H. Ramanan, K. Laubernds, S. L. Suib, M. Tsapatsis, S. L. Brock, M. Marquez, *Angew. Chem. Int. Edit.* **2003**, *42*, 2905.
[77] M. Abkarian, J. Nunes, H. A. Stone, *J. Am. Chem. Soc.* **2004**, *126*, 5978.
[78] N. L. Liu, Y. Zhou, L. Wang, J. B. Peng, J. A. Wang, J. A. Pei, Y. Cao, *Langmuir* **2009**, *25*, 665.
[79] C. Y. Zhang, X. J. Zhang, X. H. Zhang, X. Fan, J. S. Jie, J. C. Chang, C. S. Lee, W. J. Zhang, S. T. Lee, *Adv. Mater.* **2008**, *20*, 1716.
[80] L. Q. Li, P. Gao, K. C. Schuermann, S. Ostendorp, W. C. Wang, C. A. Du, Y. Lei, H. Fuchs, L. De Cola, K. Mullen, L. F. Chi, *J. Am. Chem. Soc.* **2010**, *132*, 8807.
[81] X. D. Chen, S. Lenhert, M. Hirtz, N. Lu, H. Fuchs, L. F. Chi, *Acc. Chem. Res.* **2007**, *40*, 393.
[82] S. Jin, D. M. Whang, M. C. McAlpine, R. S. Friedman, Y. Wu, C. M. Lieber, *Nano Lett.* **2004**, *4*, 915.
[83] N. Lu, J. W. Zheng, M. Gleiche, H. Fuchs, L. F. Chi, O. Vidoni, T. Reuter, G. Schmid, *Nano Lett.* **2002**, *2*, 1097.
[84] D. Whang, S. Jin, Y. Wu, C. M. Lieber, *Nano Lett.* **2003**, *3*, 1255.
[85] D. Whang, S. Jin, C. M. Lieber, *Nano Lett.* **2003**, *3*, 951.

Received: September 15, 2011
Published online: January 27, 2012

